Periodica Polytechnica Civil Engineering, 69(2), pp. 664–675, 2025

Neural Network Modeling and Sensitivity Analysis of Factors Influencing Dynamic Compaction Vibration Velocity

Jianmin Zhu[1*], Jianguo Zheng[2], Yongtang Yu[3], Baozhi Dong[4], Yuguo Wang[5], Weiwei Zhang[5]

[1] School of Civil Engineering, Xi'an University of Architecture and Technology, Xi'an 710055, China
[2] China JiKan Research Institute of Engineering Investigations and Design, Co., Ltd., Xi'an 710021, China
[3] China United Northwest Institue for Engineering Design & Research Co., Ltd., Xi'an 710077, China
[4] Jin Baodao Foundation Engineering Co., Ltd., Taiyuan 030031, China
[5] School of Institute for Interdisciplinary and Innovate Research, Xi'an University of Architecture and Technology, Xi'an 710055, China
[*] Corresponding author, e-mail: zjm1995triumph@xauat.edu.cn

Received: 25 July 2024, Accepted: 20 February 2025, Published online: 18 March 2025

Abstract
Dynamic compaction vibrations (DCV) cause significant environmental impacts. Quantifying key influencing factors is essential for mitigation. This study examines how tamper radius, tamping energy, tamping times, and tamping settlement affect DCV velocity (4000-25000 kN·m energy range) in a miscellaneous fill site. A BP neural network model was developed with these four parameters as inputs and vibration velocity as output, and the influence of each factor on vibration velocity was evaluated in combination with Sobol sensitivity analysis. The results show that Vibration velocity and tamper radius follow a negative exponential power function relationship. 97% of total vibration attenuation occurs within a 60 m radius. Vibration velocity growth rate decelerates with increasing tamping energy. 98% of velocities are below 30 mm/s, demonstrating strong data clustering. With the increase of tamping times or tamping settlement, the vibration velocity first rises to the "peak point", and the peak point corresponds to 4-6 tamping times and tamping settlement at 0.68-0.82 m and 3.08-4.30 m, and then declines or stabilizes. The tamper radius is the main factor affecting the vibration velocity. Optimizing or controlling the tamper radius can significantly reduce the vibration of DCV. The influence of tamping settlement is second, and the tamping energy and tamping times have a smaller impact.

Keywords
miscellaneous fill, dynamic compaction, vibration velocity, BP neural network, Sobol sensitivity analysis

1 Introduction

The dynamic compaction is a foundation treatment technique that uses tamping energy and shock waves to rapidly improve foundation strength, soil compaction, and eliminate collapsibility. It offers notable advantages in cost-effectiveness, efficiency, and convenience [1, 2]. Currently, it finds widespread application in various sectors, including construction [3], transportation [4], port development [5, 6], reclamation projects [7, 8], and more. However, the construction process of dynamic compaction is often accompanied by substantial energy conversion and the generation of powerful vibration waves, which can significantly impact nearby structures, construction personnel, and residents [9, 10].

It is widely accepted that the primary frequency of dynamic compaction vibrations typically falls within the range of 5–20Hz [11, 12] representing low-frequency vibrations. This frequency range aligns with the natural vibration frequency of buildings, potentially inducing a 'resonance' effect [13]. Consequently, numerous scholars have extensively investigated the influence patterns of dynamic compaction vibrations. For instance, Li and Sun [14] examined the correlation between vibration acceleration and tamping energy, soil characteristics, and distance from the tamping point in an artificial filling site based on the measured results of vibration acceleration under a tamping energy of 3768kN·m. Concurrently, the vibration isolation efficacy of the vibration isolation trench was confirmed through the analysis of vibration acceleration. Wu et al. [15] conducted a comprehensive examination of the impact of tamping times and compaction duration on velocity, spectrum waveform, peak ground velocity (PGV), peak ground acceleration (PGA),

Cite this article as: Zhu, J., Zheng, J., Yu, Y., Dong, B., Wang, Y., Zhang, W. "Neural Network Modeling and Sensitivity Analysis of Factors Influencing Dynamic Compaction Vibration Velocity", Periodica Polytechnica Civil Engineering, 69(2), pp. 664–675, 2025. https://doi.org/10.3311/PPci.37967

and average frequency under an energy level of 3200 kN·m in a stone foundation treatment project. The study revealed that the decay pattern of PGV and PGA in the all-rock foundation follows the power law with negative exponents with distance. An et al. [16] and Wiss [17] analyzed the attenuation patterns of maximum ground surface vibration velocity with propagation distance, employing tamping energies of 6000 kN·m and 43.39 kN·m, respectively. Both studies revealed a consistent adherence to the power-function relationship. Assessments of safety distances for adjacent structures were made by integrating measured data.

Applying a similarity criterion, Wu et al. [12] and Wei et al. [18] delved into the propagation and evolution of vibration velocity and waveforms under tamping energies of 1000 kN·m and 1171 kN·m based on test results of soil-rock mixture filling sites. Their analysis included exploring the vibration response of internal particles within the soil-rock filling body and examining the dynamic compaction reinforcement mechanism. Applying the principles of similarity theory, Gong et al. [19] conducted indoor model tests to examine the deformation characteristics and dynamic response features of slopes under tamping energy ranging from 3000 to 12000 kN·m. Their investigation explored the impact range of dynamic compaction on slopes. Ghanbari Alamooti and Hamidi [20] investigated the impact of distance on the peak particle velocity and peak particle displacement of slope test points through numerical simulation. Their findings indicated a reduction in both parameters as the distance increased. Taking a unique approach, Pasdarpour et al. [21] employed genetic algorithms and a fuzzy system to systematically analyze the influence of tamper weight, height of tamper drop, print spacing, tamper radius, number of impact and soil layer geotechnical properties on the efficacy of dynamic compaction. This study stands out from previous research by comprehensively considering the combined impact of multiple factors on dynamic compaction effectiveness, marking a significant contribution to dynamic compaction construction practices.

The preceding analysis shows that the soil at the site exhibits relative uniformity, whereas the soil uniformity at the miscellaneous fill site is subpar. This disparity will inevitably result in variations between dynamic compaction vibrations and those of the uniform soil site. Limited field studies have been conducted on the factors impacting the propagation of ultra-high-level vibrations. These studies have predominantly focused on the influence of individual factors on vibration velocity, making it challenging to determine the primary influencing factor of vibration response. Additionally, the observed results and patterns of the dynamic response to ultra-high-level vibrations on slopes are relatively inconclusive.

Research studies [22, 23] with statistical analysis indicate that significant damage is associated with particle velocity, whereas minor damage is linked to acceleration. Therefore, it is a prevailing practice to substitute particle velocity for particle acceleration when predicting damage potential. Therefore, the vibration speed is taken as the research object.

This study focuses on a miscellaneous fill site, exploring the impact of various factors such as tamper radius, tamping energy, tamping times, and tamping settlement on vibration velocity under tamping energy of 25000 kN·m, 12000 kN·m, and 4000 kN·m. Subsequently, the Fisher-Yates random shuffling algorithm was employed to sort the data randomly based on different factors and their corresponding vibration velocities, and input it into the Bp neural network model for regression training. The regression model is used to perform Sobol sensitivity analysis, which accurately quantifies the relative importance of each influencing factor. This method effectively determines the primary controlling factors governing vibration velocity in dynamic compaction construction. The research outcomes aim to serve as a valuable reference for dynamic compaction vibration control in similar projects.

2 Dynamic compaction vibration test

2.1 Site overview

The survey site is situated in Yinying Town, on the outskirts of Yangquan City, Shanxi Province, with coordinates at 113°34'35.0" E, 37°58'39.9" N, as shown in Fig. 1. It is an electrochemical energy storage power station affiliated with a power plant boasting a project scale of 500 MW–1000 MWh. No visible surface water was evident during the survey.

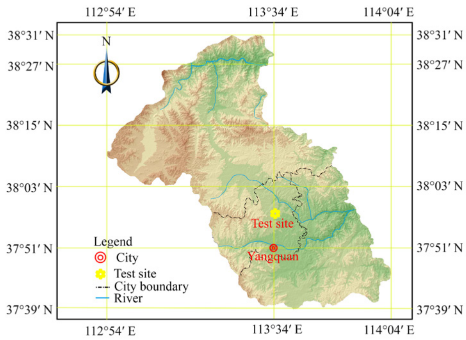

Fig.1 Geographical location of the test site

Examining specific stratigraphic sections, as depicted in Fig. 2, reveals a sequence of miscellaneous fill (Q_4^{ml}) 1 and sandy shale (C) 2 from top to bottom. The miscellaneous fill is widely dispersed across the site, displaying variegated and slightly damp characteristics. Comprising mainly gravel and cinder, it incorporates cohesive soil and coal ash. The gravel composition primarily consists of sandstone, shale, mudstone, and limestone, exhibiting varying sizes and containing a small quantity of block stone. The structure is loose to slightly densely packed, showcasing poor uniformity and stability. Backfill thickness fluctuates with terrain variations, with an average thickness of 13.58 m. Sandy shale (C) exhibits hues ranging from grayish black to grayish green, featuring a sandy structure and layered composition. The rock core is fragmented, occasionally forming short columnar structures, with the local inclusion of thin mudstone. The rock mass is soft, displaying fractures encountered during the investigation process. Table 1 presents the physical indicators, indicating average values.

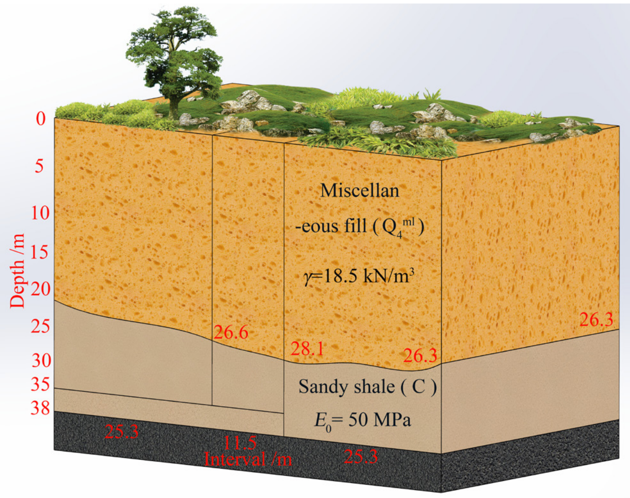

Fig. 2 Stratigraphic profile

Table 1 Physical parameters of rock and soil mass

Physical parameters	Miscellaneous fill 1	Sandy shale 2
γ/(kN/m³)	18.5	/
Number of dynamic penetrations $N_{63.5}$	7.4	/
Single axis compressive strength (MPa)	0.07	13.42
Rock quality designation (RQD)	/	20~30
Rock quality grade	/	IV
Bearing capacity f_a (kPa)	/	600
Modulus of deformation E_0 / (MPa)	/	50

2.2 Test scheme

Three survey lines were laid out in the flat field of the site, The relative positioning of the tampering point and check point is shown in Fig. 3.

The dynamic tamping energy are 25000 kN·m, 12000 kN·m, and 4000 kN·m, respectively. Each tamping energy corresponds to a survey line, with adjacent lines spaced 8 m apart. Each line features 8 checkpoints set at intervals of 10 m, 20 m, 30 m, 40 m, 60 m, 80 m, 85 m, and 90 m from the tampering point.

The number of tamping times ranged from 9 to 12. The statistics of the tamping point, checkpoint and rammer parameters are shown in Table 2.

The tampering and checkpoints are strategically arranged based on the site plan to ensure monitoring reliability. Once coordinates are determined, Real-time kinematic (RTK) positioning system is employed to produce a precise layout. The dynamic compaction vibration test is depicted in Fig. 4

2.3 Instrument and test principle

The testing apparatus includes a triaxial velocity sensor, data acquisition device, as shown in Fig. 5. The triaxial velocity sensor operates as a vector sensor, utilizing vector synthesis principles to depict point motion states precisely. It effectively captures acceleration signals even when the motion direction is unknown. Before testing, ensure the sensor securely attaches to the measured object, orienting the side with the coordinate mark upwards and perpendicular to the plumb line. Align the X or Y axis with the tamping point's center for optimal alignment.

The data acquisition device can gather and store vibration signals from the triaxial velocity sensor, allowing for

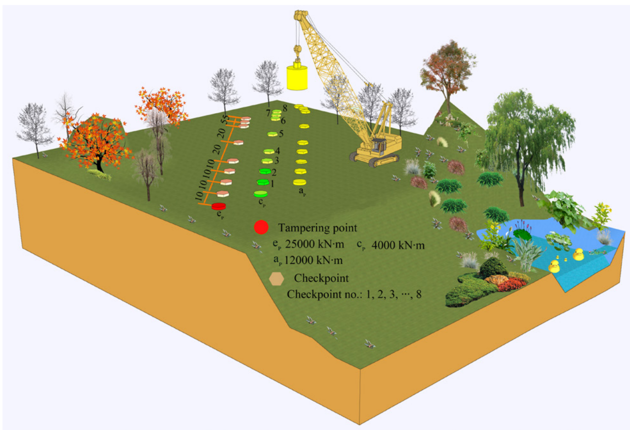

Fig. 3 Tamping and check point arrangement of test area

Table 2 Statistics of the tamping point, checkpoint and rammer parameters

Tamping energy / kN·m	Tamping point code	Checkpoint	Rammer parameters		
			Tamper diameter /m	Tamper mass / tonnes	Falling height /m
25000	e_p	e_p-(1~8)	2.4	138	18
12000	a_p	a_p-(1~8)	2.4	67	18
4000	c_p	c_p-(1~8)	2.4	25	16

Fig. 4 Dynamic compaction vibration test

Fig. 5 Vibration vibrometer

customization of acquisition parameters. Its operational range spans ±35 mm/s, with recording and reading accuracy rated at 0.1 mm/s and 0.001, respectively. It maintains high precision across temperatures ranging from −10 to 75 °C. The vibration trigger threshold is set to 20% of the peak amplitude of the measured signal to reduce the false trigger caused by non-test factors.

3 Test results and analysis

The distribution range of the master vibration frequency during the dynamic compaction construction process is shown in Fig. 6. The shaded area in the figure represents the density of data distribution. The larger the area, the larger the data volume. As can be seen from the figure, when the tamping energy is 4000 kN·m, 12000 kN·m, and 25000 kN·m, the mean of the master vibration frequency is 14.88, 10.95, and 11.72 Hz, respectively, and the standard deviation is 2.4, 2.0, and 3.8, respectively. According to the mean value ± 1 times the standard deviation, the vibration velocity statistics of the energy levels of 4000 kN·m, 12000 kN·m, and 25000 kN·m account for 68%, which are 12.52~17.24, 8.95~12.95, and 7.92~15.52 Hz, respectively. Overall, the master vibration frequency under each tamping energy is usually between 7 and 18 Hz, but with the increase of tamping energy, the mean of the master vibration frequency shows a trend of decreasing first and then increasing. The standard deviation of the data under 12000 kN·m is small, the data concentration is the highest, and the stability of the vibration frequency is high.

3.1 Influence of tamper radius on vibration velocity

The influence of tamper radius (the distance between checkpoint and tampering point) on the vibration velocity is shown in Fig. 7.

The correlation between vibration velocity and vibration tamper radius exhibits a power function relationship with a negative exponent. As the tamper radius gradually increases,

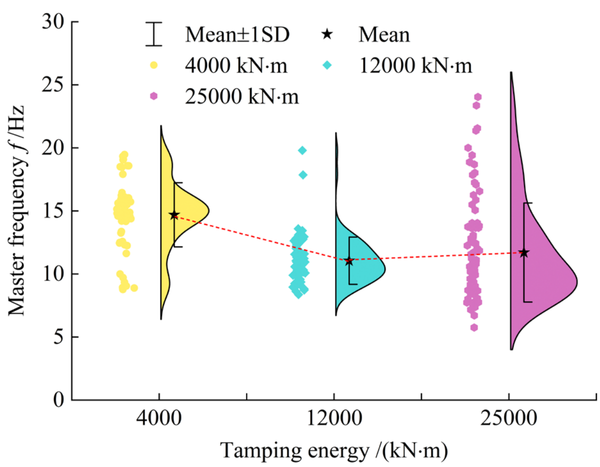

Fig. 6 Master frequency distribution

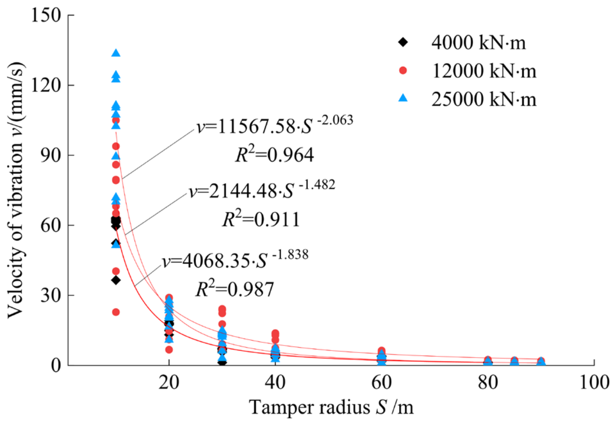

Fig. 7 The influence of tamper radius on vibration velocity

the attenuation of vibration velocity displays characteristics of rapid attenuation in proximity and slower attenuation at a greater distance. The total attenuation of vibration velocity Δv is the vibration velocity at the tamper radius of 10 m minus the vibration velocity at the tamper radius of 90 m, $v_{10} - v_{20}$ is the relative attenuation at 20 m; is the relative attenuation at 30 m; $v_x - v_y$ is the relative attenuation at the tamper radius of y m; $F = (v_x - v_y)/\Delta v$ is the relative vibration velocity decay rate. Specifically, within the distance range of 10 to 20 m, the attenuation of vibration velocity under tamping energy of 4000 kN·m, 12000 kN·m, and 25000 kN·m constitutes over 68% of the total attenuation. Extending the distance range to 10 to 60 m encompasses more than 97% of the total attenuation, signifying a rapid attenuation of dynamic compaction vibration within a 40 m radius from the tampering point. Outside this range, the influence of dynamic compaction vibration is less than 3%, and the corresponding attenuation rate is listed in Table 3.

According to the *Standard for allowable vibration of building engineering* [24], the allowable vibration velocity of building (Structure) is determined by linear interpolation based on frequency. Industrial buildings, public buildings (Grade A) and residential buildings are sensitive to vibration and have protective value (Grade B). If they do not belong to the first two categories, they belong to Grade C. Table 4 lists the safe distances between the top floor and the foundation of the building when the tamping energy is 4000, 12000 and 25000 kN·m.

Table 4 reveal that the safety distance is not directly proportional to the tamping energy. Interestingly, the safety distance under 4000 and 25000 kN·m tamping energy is identical, while the safety distance under the 12000 kN·m tamping energy surpasses that of both 4000 and 25000 kN·m.

3.2 Influence of tamping times on vibration velocity

The influence of tamping times on vibration velocity under the tamping energy of 4000, 12000, and 25000 kN·m is depicted in Fig. 8. Overall, the vibration velocity under the tamping energy of 4000, 12000, and 25000 kN·m underwent a phase of rapid increase followed by stabilization with an increase in the tamping times.

At a tamping energy of 4000 kN·m and a tamper radius of 10 m, the vibration velocity curve experiences rapid growth initially, peaking at the sixth strike, followed by a declining trend. Similarly, the curve trends at the tamper radius of 20 m, 30 m, and 40 m from the tamping source are generally similar, stabilizing after the peak value of the fourth strike. Notably, the vibration velocity at 60 and 80 m does not increase significantly with the tamping times. At a tamping energy of 12000 kN·m and a tamper

Table 4 Safety distance

Tamping energy /kN·m	Top floor/m			Foundation /m		
	A	B	C	A	B	C
4000	40	60	60	30	40	60
12000	60	80	80	30	60	80
25000	40	60	60	30	40	60

Table 3 The influence law of tamper radius on vibration velocity attenuation rate

S/m	4000 kN·m			12000 kN·m			25000 kN·m		
	v/(mm/s)	Δv/(mm/s)	F %	v/(mm/s)	Δv/(mm/s)	F %	v/(mm/s)	Δv/(mm/s)	F %
10	55.3	-	-	65.2	-	-	111.50	-	-
20	16.0	39.3	72.50	21.6	43.5	68.88	22.30	89.2	80.47
30	7.70	8.20	15.22	11.4	10.3	16.28	8.70	13.6	12.28
40	4.60	3.10	5.74	7.20	4.2	6.60	4.50	4.20	3.83
60	2.20	2.40	4.40	3.80	3.4	5.41	1.70	2.80	2.46
80	1.30	0.90	1.66	2.40	1.4	2.19	0.90	0.80	0.77
85	1.20	0.10	0.25	2.20	0.2	0.35	0.80	0.10	0.11
90	1.10	0.10	0.22	2.00	0.2	0.30	0.70	0.10	0.09

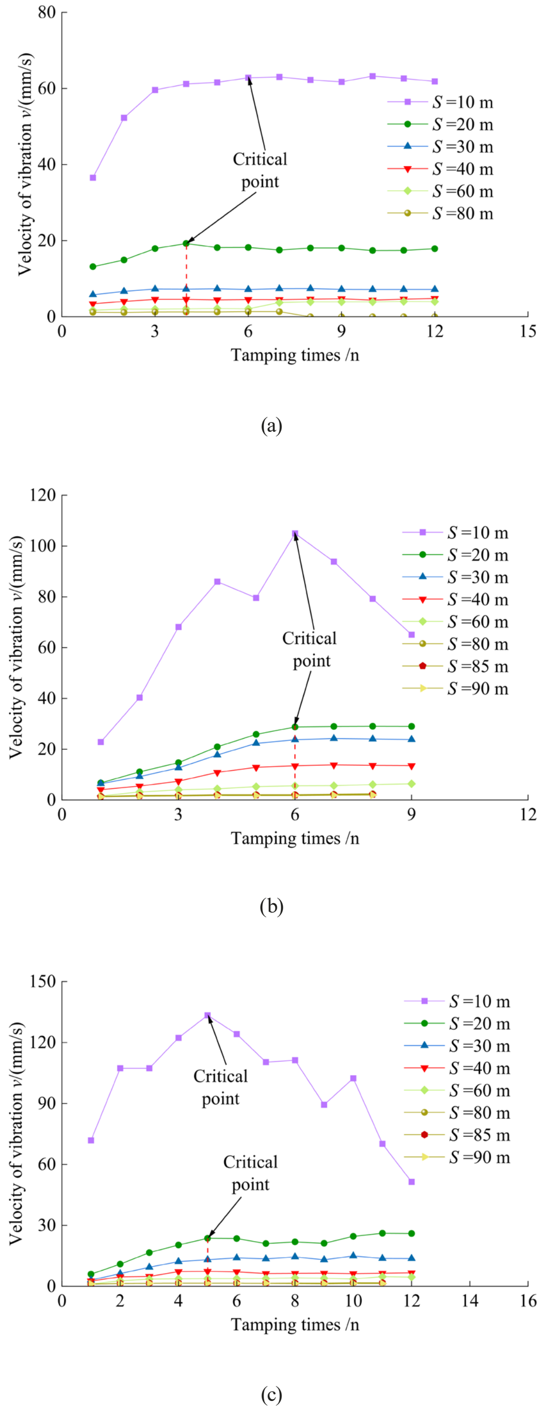

Fig. 8 The influence of tamping times on vibration velocity: (a) 4000 kN·m, (b) 12000 kN·m, (c) 25000 kN·m

radius of 10 m, the curve exhibits an ascending trend with an increase in the tamping times. The curve at the tamper radius of 20 m, 30 m, and 40 m stabilizes after reaching the peak value at the sixth strike. Similarly, the curve trends at 60 m, 80 m, 85 m, and 90 m are relatively stable, with the vibration speed showing no significant change with an increase in the tamping times. At a tamping energy of 25000 kN·m and a tamper radius of 10 m, the curve experiences rapid growth initially with an increase in the tamping times. It then shows a downward trend after its peak at the fifth strike. When the tamper radius is 20 m, except for the first strike, the curve generally increases first and then tends to stabilize, reaching its peak at the fifth strike. The curve at 30 m and 40 m from the tamping point tends to stabilize after the peak value of the fifth strike. The curve trends at 60 m, 80 m, 85 m, and 90 m are relatively stable, with the vibration speed showing no significant change with an increase in the tamping times.

There is a distinct stable 'critical point' in the impact of tamping times on the vibration velocity of dynamic compaction. Specifically, the 'critical point' for 4000 kN·m is at 10 m, with six strokes as the critical point, and at 20 m, 30 m, and 40 m, with four strokes as the critical point; for 12000 kN·m, the critical point is at the sixth stroke; for 25000 kN·m, the fifth strike is the critical point. Identifying the critical points of tamping times can guide controlling dynamic compaction vibration.

3.3 Influence of tamping energy on vibration velocity

The three-dimensional maximum vibration velocity distribution under the tamping energy of 4000, 12000, and 25000 kN·m is shown in Fig. 9. Under the tamping energy of 4000 kN·m, 12000 kN·m, and 25000 kN·m., the average values of the maximum vibration velocity are 16.32 mm/s, 17.12 mm/s and 19.11 mm/s respectively, indicating that with the increase of dynamic tamping energy level, the average value of maximum vibration velocity under each energy level does not change much. Under varying energy levels, a discernible threshold demarcates the aggregation characteristics of vibration velocity data. When the

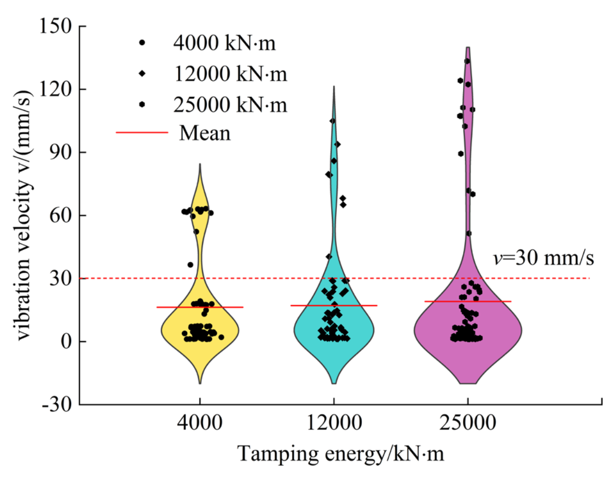

Fig. 9 Vibration velocity distribution

vibration velocity exceeds 30 mm/s, pronounced dispersion is observed among the measured values, whereas velocities at or below 30 mm/s exhibit significant clustering patterns. Statistical analysis indicates that vibration velocities ≤30 mm/s account for 98% of the total sample population, demonstrating a concentrated distribution characteristic.

The vibration velocity survey data of dynamic compaction are analyzed according to the boundary of 30 mm/s aggregation degree, as shown in Fig. 10. The maximum vibration velocity under each energy level is connected, and the growth rate Line 1 of vibration velocity with the increase of energy level is obtained. Connect the maximum vibration velocity in the data sample less than or equal to 30 mm/s, and get the broken Line 2 of the vibration velocity growth rate. Line 1 and Line 2 indicate that the vibration velocity increases with rising tamping energy. The change rate of maximum vibration velocity is 0.529% when the energy level increases from 4000 kN·m to 12000 kN·m, and 0.219% when the energy level increases from 12000 kN·m to 25000 kN·m, with the former being more than twice that of the latter. However, when the vibration velocity is less than 30 mm/s, the maximum change rate of vibration velocity is 0.119% when the energy level is from 4000 kN·m to 12000 kN·m, and the change rate is −0.007% when the energy level is from 12000 kN·m to 25000 kN·m, showing a decreasing trend, indicating that with the increase of tamping energy, there is an inflection point in the growth rate of vibration velocity at 12000 kN·m.

3.4 Influence of tamping settlement on vibration velocity

The influence of tamping settlement on vibration velocity is depicted in Fig. 11(a)–(c). The vibration velocity shows a trend of first rapid growth and then stabilization with the

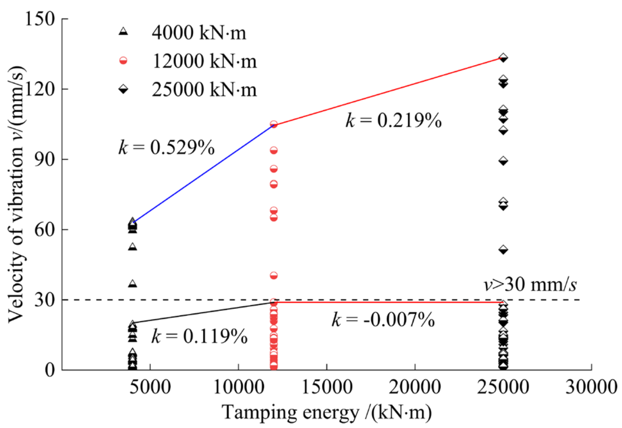

Fig. 10 The influence of tamping energy on vibration velocity

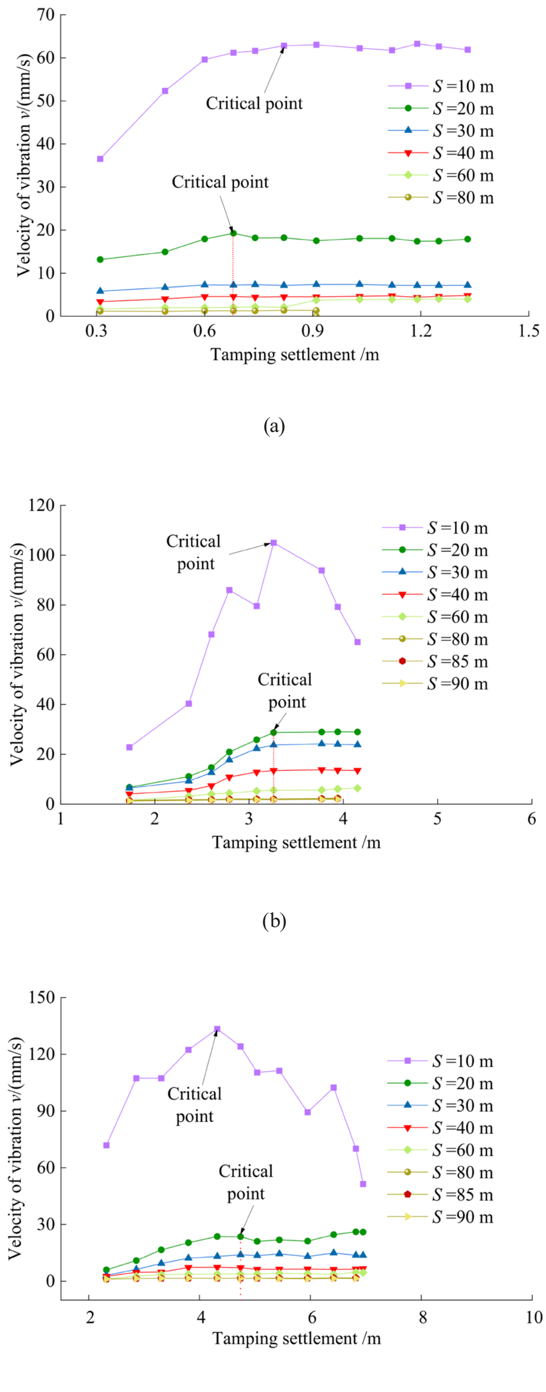

Fig. 11 The influence of tamping settlement on vibration velocity: (a) 4000 kN·m, (b) 12000 kN·m, (c) 25000 kN·m

increase of cumulative tamping amount. When the compaction energy is 4000 kN·m and the compaction radius is 10 m, the vibration velocity reaches a peak value at a cumulative settlement of 0.82 m and then fluctuates slightly, and tends to be stable overall; when the compaction radius is 20 m, 30 m, and 40 m, the vibration velocity reaches a maximum value at a cumulative settlement of about

0.68 m and tends to be stable, and the vibration velocity at 60 m and 80m changes little. When the tamping energy is 12000 kN·m and 25000 kN·m, as the cumulative tamping amount increases, the vibration velocity tends to be stable after reaching the maximum value, and the cumulative tamping amount corresponding to the maximum value of the vibration velocity is generally 3.08 m to 4.30 m.

Research indicates that [25] dynamic compaction vibrations disperse outward from the hammer's bottom and sides through elastic wave propagation. Analysis of the dynamic compaction process reveals a progressive decrease in settlement amounts during initial blows, accompanied by a transition in soil consistency from soft to hard. Soft soil can absorb some of the vibration energy, resulting in relatively low vibration velocities at ground test points during this phase. As soil settlement under the hammer diminishes and the soil continues to harden, the soil's ability to absorb vibration energy decreases, leading to increased vibration velocities at ground points. Subsequent hammering leads to slow increases in settlement and pit depth and a continuous increase in the distance between the test point and the hammer's center. This increased distance weakens the propagation of vibration energy. At the tamping energy of 4000 kN·m, where the rammer's weight is light, settlement increments per tamping are small, with minimal impact on vibration velocity, especially with enhanced elastic wave effects on the rammer's side. Conversely, settlement increases rapidly at the compaction energies of 12000 kN·m and 25000 kN·m, leading to a notable impact of pit depth on vibration velocity, particularly at 10 meters. At distances between the tamping point ranging from 20 to 90 m, side elastic waves from the hammer significantly influence vibration velocity, resulting in relatively stable readings.

4 Sobol sensitivity analysis

The studies mentioned above only examined the impact of individual factors, such as tamping energy, tamper radius, tamping times, and cumulative tamping settlement, on vibration velocity. However, determining the combined effects of multiple factors on vibration velocity remains challenging, and even more difficult is establishing the relative significance of each factor. As a result, it becomes hard to provide systematic guidance for the design and construction of dynamic tamping vibration reduction.

Sobol sensitivity analysis is a Monte Carlo method based on variance decomposition [26]. The principle involves decomposing the model into single parameters based on two and an increasing sequence function composed of parameters. Subsequently, the influence of the variance of the single parameter and the combined parameter on the total variance is calculated to assess the importance of the parameter, thus deriving the sensitivity method [27]. Sobol sensitivity analysis comprises sensitivity indicators such as the local sensitivity index and the total effect index. The local sensitivity index reflects the influence of a single parameter on the output. A larger index indicates a greater parameter influence on the output. The total effect index is used to measure the total contribution of the model input parameter to the variance of the output result, including the independent effect of the parameter and all its interactions with other parameters [28].

Assume that the functional relationship of the model is $y = f(x)$ where $x = (x_1, x_2, \ldots, x_n)$, with 'n' representing the n-dimensional input, and y is the output. The model $y = f(x)$ is decomposed into the sum of n increasing terms based on 2:

$$\begin{aligned} f(x) = f_0 + \sum_{i=1}^{n} f_i(x_i) + \sum_{1\le i<j\le n} f_{i,j}(x_i, x_j) + \\ \ldots + f_{1,2,\ldots n}(x_1, x_2, \ldots x_n) \end{aligned} \tag{1}$$

$$f_0 = E(y) = \int f(x)\,dx \tag{2}$$

$$f_i = E(y/x_i) - f_0 = \int f(x) \prod_{z\ne i} dx_z - f_0 \tag{3}$$

$$\begin{aligned} f_{i,j} &= E(y/x_i, x_j) - f_i - f_j - f_0 \\ &= \int f(x) \prod_{z\ne i,j} dx_z - f_i - f_j - f_0 \end{aligned} \tag{4}$$

Then the total variance of function $f(x)$ is:

$$D = \int f^2(x)\,dx - f_0^2 \tag{5}$$

The deviation is

$$\begin{aligned} &D_{i_1,i_2,\ldots,i_z} = \int f^2_{i_1,i_2,\ldots,i_z}(x_{i_1}, x_{i_2}, \ldots, x_{i_z})\,dx_{i_1}dx_{i_2}\ldots dx_{i_z} \\ &1 \le i_1 < \ldots < i_z \le n,\ \ z = 1, 2, \ldots n \end{aligned} \tag{6}$$

Then the total variance of function $f(x)$ is:

$$S_{i_1,i_2,\ldots,i_z} = \frac{D_{i_1,i_2,\ldots,i_z}}{D} \tag{7}$$

When $z = i$, the main influence of the parameter x_i on the output $f(x)$ is represented.

When conducting multi-factor analysis, it is very complex to establish a multivariate nonlinear model $f(x)$ including the vibration source distance S, the number of tamping times N, the tamping energy E, the tamping settlement J and the vibration velocity v. Based on the universal function approximation characteristics of the BP neural network (Back Propagation Neural Network) [29], this study will use the BP neural network to construct the *S*-*N*-*E*-*J*-*v* mapping relationship model. A total of 217 sets of vibration data were collected on site, covering tamping energy of 4000, 12000, and 25000 kN·m, vibration source distances of 10, 20, 30, 40, 60, 80, 85, and 90 m, tamping times (1, 2, 3, ...), and settlement amounts of 220 mm to 6740 mm. In order to reduce the influence of the original data arrangement order on the modeling accuracy, the Fisher-Yates random shuffling algorithm [30] was used to randomly sort the data to disrupt the correlation between the original adjacent data rows.

The BP neural network training and Sobol sensitivity analysis process are shown in Fig. 12. The 217 data sets were divided into "training group G" and "prediction group H". In the training stage, the optimal structural parameters were determined by experimental method: single hidden layer architecture with 7 nodes and initial learning rate of 0.01. Taking the "G/H = 180:37" group as an example, the training used the adaptive moment estimation optimizer (Adam). When the loss function of the validation set decreased by less than 10^{-6} for 1000 consecutive iterations, the early stopping mechanism was triggered, and the training was completed after 42 iterations. Table 5 lists the simulation accuracy of different training groups and prediction groups. When "G/H = 180:37", the MAE (mean absolute error), MBE (mean deviation error) and RMSE (root mean square error) of the model were relatively small, and the coefficient of determination R^2 was as high as 0.98. Save the

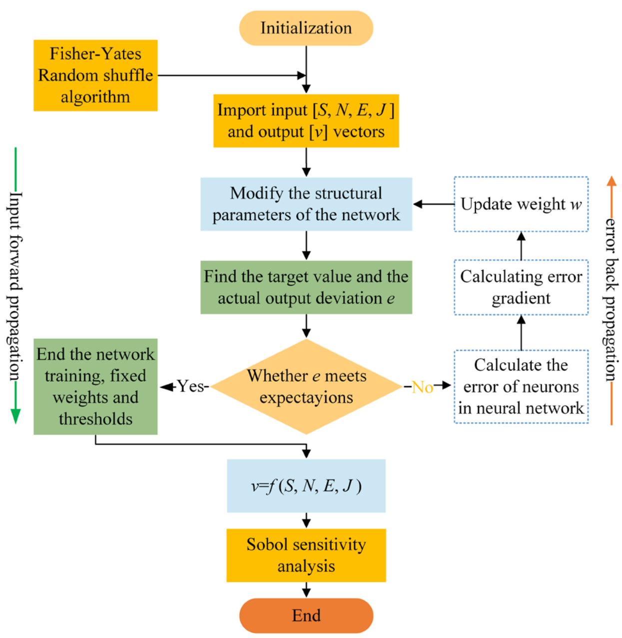

Fig. 12 BP neural network modeling and Sobol sensitivity analysis

Table 5 The influence of the ratio of training group to prediction group on the accuracy of the model

G/H	R^2		MAE		MBE		RMSE	
	G	H	G	H	G	H	G	H
100:117	0.82	0.77	0.62	0.66	−0.15	−0.28	1.04	1.37
120:97	0.73	0.62	0.77	0.86	−0.10	−0.29	1.32	1.78
140:77	0.92	0.86	0.35	0.50	−0.13	−0.31	0.72	1.13
160:57	0.89	0.84	0.33	0.50	−0.11	−0.26	0.80	1.31
180:37	0.98	0.98	0.23	0.26	−0.09	−0.12	0.35	0.44
190:27	0.95	0.96	0.34	0.41	−0.02	−0.12	0.58	0.60

"G/H = 180:37" group model. Figs. 13(a) and 13(b) show the training and prediction effects of the model, respectively.

After calculation, the sensitivity indexes of various factors affecting dynamic compaction vibration were determined, as shown in Table 6. The sensitivity histogram of tamping energy, tamper radius, tamping times, and tamping settlement to vibration velocity is shown in Fig. 14.

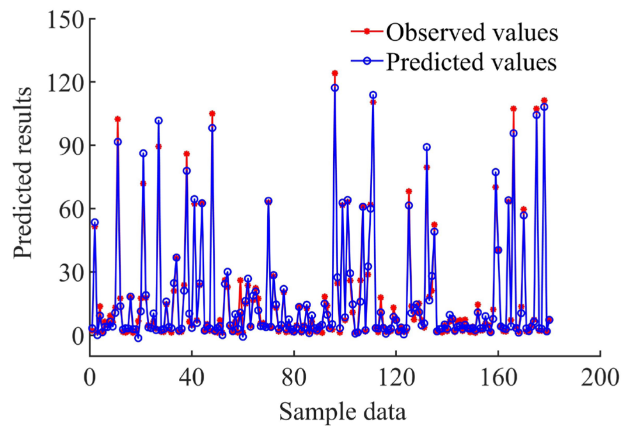

(a)

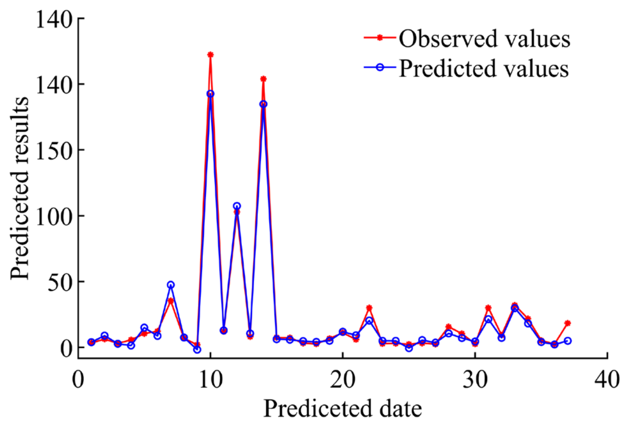

(b)

Fig. 13 Bp neural network model at A:B = 180:37: (a) Training samples and observed values, (b) predicted date and observed date

Table 6 Sensitivity index of dynamic compaction construction parameters

Variable number	Variable	Local sensitivity index SL	Total sensitivity index ST
1	Tamping energy	0.0043	0.0206
2	Tamper radius	0.5974	0.8229
3	Tamping times	0.0130	0.0466
4	Tamping settlement	0.1352	0.3721

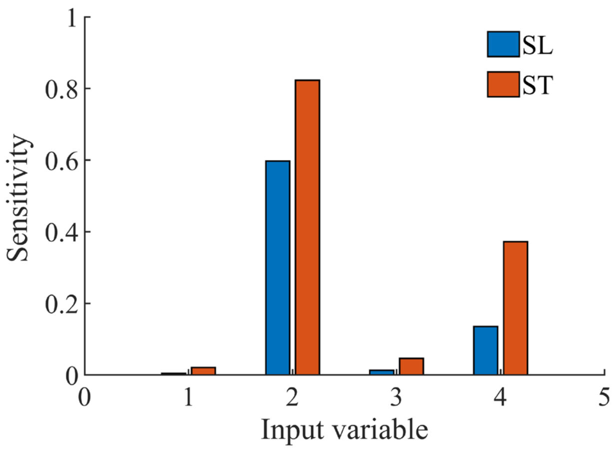

Fig. 14 Sensitivity indicators

From Table 6 and Fig. 14, it can be seen that the sensitivity of vibration velocity to tamping energy, tamper radius, tamping times, and tamping settlement is ranked as follows:

Tamper radius > Tamping settlement > Tamping times > Tamping energy

Table 6 demonstrate that the local sensitivity index (SL) of the tamper radius on vibration velocity is 138.93 times higher than that of tamping energy and 46 times higher than that of tamping times. The total effect index (ST) for the tamper radius is 39.9 times that of tamping energy and 17.7 times that of tamping times, indicating that the tamper radius not only significantly contributes to vibration velocity but also interacts notably with other variables. Tamping settlement ranks second, with an SL 31.4 times that of tamping energy and 10.4 times that of tamping times, and an ST 18.1 times that of tamping energy and 7.98 times that of tamping times. In contrast, the sensitivities of tamping energy and tamping times are relatively low, indicating their minimal impact on vibration velocity.

The above research shows that the tamper radius is the main factor affecting the vibration velocity. Its optimization or control can significantly reduce the vibration of strong compaction; the impact of tamping settlement is second, which needs to be paid attention to in design or construction; the tamping energy and tamping times have little impact and can be regarded as secondary factors of concern.

The research indicates that the tamper radius is the primary factor affecting vibration velocity. Optimizing or controlling it can significantly reduce vibrations. Tamping settlement has a less significant impact and should be considered during design and construction. In comparison, tamping energy and tamping times have minimal effects and can be considered secondary factors.

5 Conclusions

In this study, the influence of four factors-namely tamping energy, tamper radius, tamping times, and tamping settlement-on vibration velocity at 25000 kN·m, 12000 kN·m, and 4000 kN·m was investigated at a miscellaneous fill site. A nonlinear model of the relationship between these four factors and vibration velocity was established using a BP neural network. The Sobol sensitivity analysis method was employed to determine the order of influence of these factors on dynamic tamping vibration velocity. The following conclusions were drawn:

1. The vibration velocity and tamper radius have a power function relationship with a negative exponent. Within a tamper radius of 60 meters, 97% of total vibration attenuation occurs, indicating a significant influence. There is a 'turning point', in the safety distance, and the safety distance decreases after exceeding the 'turning point'. From the current site test situation, the safety distance is equal when the tamping energy is 4000 kN·m and 25000 kN·m. In all kinds of buildings, the safety distance of the roof and foundation should not be less than 60 m, and when the tamping energy is 12000 kN·m, should not be less than 80 m.
2. An evident and stable 'critical point' emerges in the impact of tamping times on the dynamic compaction vibration velocity. For 4000 kN·m, when the tamper radius is 10 m, the critical point is after six strikes, and for tamper radius of 20, 30, and 40 m, the critical point is after four strikes. At 12000 kN·m, the critical point occurs at the sixth stroke, while at 25000 kN·m, the fifth strike serves as the critical point.
3. With the increase of tamping energy, the growth rate of vibration velocity changes from fast to slow. The vibration velocity of different tamping energy is concentrated below 30 mm/s, accounting for 98% of

the total data. When it exceeds 30 mm/s, the vibration velocity data is obviously dispersed.

4. The vibration velocity first increases rapidly with the increase of the cumulative tamping settlement, and then tends to be stable after reaching the peak point. When the tamping energy is 4000 kN·m, the cumulative tamping settlement corresponding to the peak point of the vibration velocity is 0.68–0.82 m. When the tamping energy is 12000 kN·m and 25000 kN·m, the cumulative tamping settlement corresponding to the peak point of the vibration velocity is 3.08–4.30 m.
5. The local sensitivity index of tamper radius on vibration velocity is 138.93 times that of tamping energy and 46 times that of tamping times. The total effect sensitivity index is 39.9 times that of tamping energy and 17.7 times that of tamping times. The local sensitivity index of tamping settlement on vibration velocity is 31.4 times that of tamping energy and 10.4 times that of tamping times, while the total effect sensitivity index is 18.1 times that of tamping energy and 7.98 times that of tamping times. Among these factors, tamper radius is the primary influence on vibration velocity. Optimizing or controlling the tamper radius can significantly reduce the intensity of tamping vibrations. Tamping settlement follows in importance, while tamping energy and tamping times have a relatively minor effect.

Acknowledgement

The project presented in this article is supported by Natural Science Foundation of China (Grant Nos. 42277151); Natural Science Foundation of China (Grant Nos. 42307277); Shaanxi Province Qin Chuangyuan "Scientist+Engineer" Team Construction Project (Grant Nos. 2022KXJ-086).

References

[1] Abedini, F., Rafiee-Dehkharghani, R., Laknejadi, K. "Mitigation of Vibrations Caused by Dynamic Compaction Considering Soil Nonlinearity", International Journal of Civil Engineering, 20(7), pp. 809–826, 2022. https://doi.org/10.1007/s40999-022-00700-9

[2] Zhang, R., Sun, Y., Song, E. "Simulation of dynamic compaction and analysis of its efficiency with the material point method", Computers and Geotechnics, 116, 103218, 2019. https://doi.org/10.1016/j.compgeo.2019.103218

[3] Liu, H., Zhao, M. "Review of ground improvement technical and its application in China", China Civil Engineering Journal, 49(1), pp. 96–115, 2016. https://doi.org/10.15951/j.tmgcxb.2016.01.012

[4] Cui, X. "Real-time diagnosis method of compaction state of subgrade during dynamic compaction", Geotechnical Testing Journal, 33(4), pp. 299–303, 2010. https://doi.org/10.1520/GTJ102268

[5] Chenaria, R. J., Farda, M. K., Sosahaba, J. S., Navarib, S. "Land Reclamation Project in Anzali Harbor Using Dynamic Compaction", Computational Research Progress in Applied Science & Engineering, 3(4), pp. 153–164, 2017.

[6] Sieradzki, M. P., Engineer S. G. "Deep dynamic compaction for subgrade improvements within the Port of Long Beach", Inżynieria Morska i Geotechnika, 2017(2), pp. 78–82, 2017.

[7] Feng, S., Shui, W., Gao, L., He, L., Tan, K. "Field studies of the effectiveness of dynamic compaction in coastal reclamation areas", Bulletin of Engineering Geology and the Environment, 69(1), pp. 129–136, 2010. https://doi.org/10.1007/s10064-009-0242-x

[8] Feng, S.-J., Tan, K., Shui, W.-H. "Dynamic Compaction of Ultra-High Energy in Combination with Ground Replacement in Coastal Reclamation Areas", Marine Georesources & Geotechnology, 33(2), pp. 109–121, 2015. https://doi.org/10.1080/1064119X.2013.805288

[9] Ghassemi, A., Pak, A., Shahir, H. "Numerical study of the coupled hydro-mechanical effects in dynamic compaction of saturated granular soils", Computers and Geotechnics, 37(1–2), pp. 10–24, 2010. https://doi.org/10.1016/j.compgeo.2009.06.009

[10] Wang, G., Yin, Y., Wang, J. "Vibration safety evaluation and vibration isolation control measures for buried oil pipelines under dynamic compaction: A case study", Soil Dynamics and Earthquake Engineering, 167, 107783, 2023. https://doi.org/10.1016/j.soildyn.2023.107783

[11] Van Impe, W. "Soil Improvement Techniques and their Evolution", CRC Press, 1989. ISBN: 978-9061918059

[12] Wu, S., Wei, Y., Zhang, Y., Cai, H., Du, J., Wang, D., Xiao, J. "Dynamic compaction of a thick soil-stone fill: Dynamic response and strengthening mechanisms", Soil Dynamics and Earthquake Engineering, 129, 105944, 2020. https://doi.org/10.1016/j.soildyn.2019.105944

[13] Nelson, F. B., Briet, S., Morel, J.-F., Lauzon, M. "Ground Vibrations Induced by Dynamic Compaction and Rapid Impact Compaction", In: 14th Pan-American Conference on Soil Mechanics and Geotechnical Engineering & 64th Canadian Geotechnical Conference, Toronto, Ontario, Canada, 2011.

[14] Li, F., Sun, Y. "Experimental research on the influence of vibration during improvement of the ground with dynamic compaction", Journal of Southeast University (Natural Science Edition), 32(5), pp. 809–812, 2002. https://doi.org/10.3321/j.issn:1001-0505.2002.05.028

[15] Wu, J., Ma, L., Shi, J., Sun, Y., Ke, J., Wang, D. "Investigation of Ground Vibration of Full-stone Foundation under Dynamic Compaction", Shock and Vibration, 2019(1), pp. 1–11, 2019. https://doi.org/10.1155/2019/2631797

[16] An, H., Xu, Z., Feng, R. "Study on the ground vibration zone during dynamic compaction for site improvement of a railway station and yard ground", Journal of Beijing Jiaotong University, 34(1), pp. 50–53, 2010. https://doi.org/10.3969/j.issn.1673-0291.2010.01.011

[17] Wiss, J. F. "Construction vibrations: State-of-the-art", Journal of the Geotechnical Engineering Division, 107(2), pp. 167–181, 1981. https://doi.org/10.1061/AJGEB6.0001095

[18] Wei, Y., Cai, H., Wu, S., Xiao, J., Song, J. "Vibration response and reinforcement mechanism of high-fill soil-stone mixtures by dynamic compaction", Chinese Journal of Geotechnical Engineering, 41(S1), pp. 237–240, 2019. https://doi.org/10.11779/CJGE2019S1060

[19] Gong, M., Cheng, Q., Liu, Z. "Model test study of dynamic responses of loess slope by dynamic compaction", Rock and Soil Mechanics, 32(7), pp. 2001–2006, 2011. https://doi.org/10.16285/j.rsm.2011.07.009

[20] Ghanbari Alamooti, E., Hamidi, A. "Stability analysis of dry sandy slopes adjacent to dynamic compaction process", Scientia Iranica, 24(1), pp. 82–95, 2017. https://doi.org/10.24200/SCI.2017.2379

[21] Pasdarpour, M., Ghazavi, M., Teshnehlab, M., Sadrnejad, S. A. "Optimal design of soil dynamic compaction using genetic algorithm and fuzzy system", Soil Dynamics and Earthquake Engineering, 29(7), pp. 1103–1112, 2009. https://doi.org/10.1016/j.soildyn.2008.09.003

[22] Hamidi, B., Nikraz, H., Varaksin, S. "Dynamic Compaction Vibration Monitoring in a Saturated Site", In: International Conference on Advances in Geotechnical Engineering, Perth Australia, 2011, pp. 267–272. ISBN: 978-0-646-55142-5

[23] Duvall, W. I., Folgelson, D. E. "Review of Criteria of Estimating Damage to Residences from Blasting Vibrations", United States Department of the Interior, Bureau of Mines, Pittsburgh, PA, USA, 5968, 1962.

[24] SAC "GB 50868-2013, Standard for allowable vibration of building engineering", The Standardization Administration of the People's Republic of China, Beijing, People's Republic of China, 2013.

[25] Miller, G. F., Pursey, H., Bullard, E. C. "On the partition of energy between elastic waves in a semi-infinite Solid", Proceedings of the Royal Society A: Mathematical and Physical Sciences, 233(1192), pp. 55–69, 1955. https://doi.org/10.1098/rspa.1955.0245

[26] Sobol, I. M. "Global sensitivity indices for nonlinear mathematical models and their Monte Carlo estimates", Mathematics and Computers Simulation, 55(1–3), pp. 271–280, 2001. https://doi.org/10.1016/S0378-4754(00)00270-6

[27] Canchila, C., Zhou, S., Song, W. "Hyperparameter Optimization and Importance Ranking in Deep Learning–Based Crack Segmentation", Journal of Computing in Civil Engineering, 38(2), 04023042, 2024. https://doi.org/10.1061/JCCEE5.CPENG-5512

[28] Brandstaeter, S., Fuchs, S. L., Biehler, J., Aydin, R. C., Wall, W. A., Cyron, C. J. "Global Sensitivity Analysis of a Homogenized Constrained Mixture Model of Arterial Growth and Remodeling", Journal of Elasticity, 145(1), pp. 191–221, 2022. https://doi.org/10.1007/s10659-021-09833-9

[29] Ahmadi, M., Naderpour, H., Kheyroddin, A. "ANN model for predicting the compressive strength of circular steel-confined concrete", International Journal of Civil Engineering, 15(2), pp. 213–221, 2017. https://doi.org/10.1007/s40999-016-0096-0

[30] Wang, X., Su, Y., Liu, L., Zhang, H., Di, S. "Color image encryption algorithm based on Fisher-Yates scrambling and DNA subsequence operation", The Visual Computer, 39(1), pp. 43–58, 2021. https://doi.org/10.1007/s00371-021-02311-2